Seventh International Conference on CFD in the Minerals and Process Industries
CSIRO, Melbourne, Australia
9-11 December 2009

Numerical investigation of the cold spray process

Shuo Li [1*] , Barry Muddle [2], Mahnaz Jahedi [3] and Julio Soria [1]

[1] Laboratory for Turbulence Research in Aerospace & Combustion, Department of Mechanical and Aerospace Engineering, Monash University, Victoria 3800, AUSTRALIA

[2] ARC Centre of Excellence for Design in Light Metals, Monash University, Victoria 3800, AUSTRALIA

[3] CSIRO Materials Science and Engineering, Clayton, Victoria 3169, AUSTRALIA

*Corresponding author, E-mail address: Shuo.Li@eng.monash.edu.au

ABSTRACT

This paper reports an investigation of the particle and gas dynamics during the cold spray process using copper particles. An overexpanded de-Laval nozzle operating at a stagnation pressure and temperature of 3.0 MPa and 900 K is used to accelerate the carrier gas. The gas dynamics are solved using a Riemann solver while the particles are tracked using a Lagrangian formulation. The accuracy of the code is assessed by comparing with experimental data for an overexpanded impinging gas jet. Streamwise and spanwise particle velocity and temperature profiles are then extracted and shown to respond very little to changes in the gas dynamics. The application of computational fluid dynamics (CFD) in locating the optimum particle impact conditions is also discussed.

NOMENCLATURE

z *jet axis*
r *radial axis*
a_e *characteristic velocity*
T_e *characteristic temperature*
ρ_e *characteristic density*
D_e *characteristic length*
$V_{i,j}$ *volume of mesh*
d_p *particle diameter*
d_m *mean particle diameter*
σ^2 *standard deviation of particle size*
f *particle size probability distribution*
g *particle size cumulative probability distribution*
η *load ratio*
N_k *number of particles in pacel k*
N_p *number of parcel per cell*
Δt *time step*
Δ *cell length*
ΔA *grid area*
u *axial velocity*
v *radial velocity*
U *velocity magnitude*
P *pressure*
ρ *density*
T *temperature*
a *speed of sound*
E *internal energy*
t *time*
P_0 *stagnation pressure*
T_0 *stagnation temperature*
C *specific heat*
τ *shear stress terms*
q *heat flux terms*
μ *dynamic viscosity*
κ *thermal conductivity*
PR *pressure ratio*
C_D *drag coefficient*
Nu *Nusselt number*
St *Stokes number*
Ma *Mach number*
Pr *Prandtl number*
Re *Reynolds number*
γ *specific heat ratio*

Subscripts

i, j *label of mesh in z and r axes*
k *particle parcel index*
e *nozzle exit*
p *particle phase*
g *gas phase*

INTRODUCTION

Cold spray is an emerging surface coating technology developed at the Institute for Theoretical and Applied Mechanics of the Siberian Division of the Russian Academy of Science by Alkimov et al. (1990). In the system shown in Figure 1, a carrier gas is pumped through a de-Laval nozzle to attain supersonic velocity. Solid powder particles are injected into the converging section of the nozzle and accelerated by the expanding gas. To achieve higher velocities, the gas is often preheated in the chamber to temperatures ranging between 800 and 1000 K. It is widely believed that given sufficient

velocity, the particles will deform upon impact and bond to the substrate. The exact physical mechanisms by which the particles deform and adhere remain the subject of ongoing research.

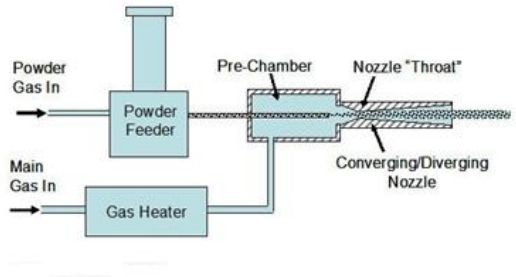

Figure 1: Schematic of typical cold spray system. [Sandia National Laboratory]

For the present study, a CFD model with coupling between the gas and particle phase as well as polydisperse particle tracking was developed. The nozzle has a throat and exit diameters of 3 mm and 8 mm respectively with converging and diverging lengths of 30 and 70mm. The nozzle chamber pressure and temperature is set at 3.0 MPa and 900 K respectively to drive the nitrogen carrier gas. These conditions result in an overerexpanded jet with pressure ratio $PR = P_{exit}/P_{ambient} = 0.2$ and Mach number $Ma = u_{exit} / a_{exit} = 4.0$. Copper particles are sprayed towards the substrate at a standoff distance of 16 mm. It's appropriate to express the particle properties in terms of the Stokes number $St = \frac{\rho a_e d_p^2}{18 \mu D_e}$ which is the ratio of the particle relaxation time and fluid characteristic time scale. The former is the time required after a step change in flow for the velocity lag $|V_f - V_g|$ to be reduced by a factor of $1/e = 0.368$. The fluid time scale is the nozzle exit diameter divided by the speed of sound at the exit. The Stokes numbers for the 4 and 8 μm particles are 17.2 and 68.7 respectively.

MODEL DESCRIPTION

For the present study, the gas flow is assumed to be laminar and axisymmetric. Despite these simplifying assumptions, it will be shown that the computed velocities for an overexpanded impinging gas jet do compare favorably with particle image velocimetry (PIV) measurements. The conservation form of the non-dimensionalised Navier-Stokes equations are written in the cylindrical system as:

$$\frac{\partial U}{\partial t}+\frac{\partial F}{\partial z}+\frac{\partial G}{\partial r}+\frac{\partial F_v}{\partial z}+\frac{\partial G_v}{\partial r}+S+S_v=0$$

where

$$U=\begin{bmatrix}\rho\\ \rho u\\ \rho v\\ E\end{bmatrix} \qquad F=\begin{bmatrix}\rho u\\ \rho u^2+P\\ \rho uv\\ (E+P)u\end{bmatrix}$$

$$G=\begin{bmatrix}\rho v\\ \rho uv\\ \rho v^2+P\\ (E+P)v\end{bmatrix} \qquad S=\frac{1}{r}\begin{bmatrix}\rho v\\ \rho uv\\ \rho v^2\\ (E+P)v\end{bmatrix}$$

$$F_v=\begin{bmatrix}0\\ \tau_{zz}\\ \tau_{zr}\\ u\tau_{zz}+v\tau_{zr}-q_z\end{bmatrix} \qquad G_v=\begin{bmatrix}0\\ \tau_{rz}\\ \tau_{rr}\\ u\tau_{rz}+v\tau_{rr}-q_r\end{bmatrix}$$

$$S_v=\frac{1}{r}\begin{bmatrix}0\\ \tau_{zr}-\frac{2}{3}r\frac{Ma}{Re}\frac{\partial}{\partial z}\left(\mu\frac{v}{r}\right)\\ \tau_{rr}-\hat{\tau}-\frac{2}{3}\frac{Ma}{Re}\frac{\partial}{\partial z}\left(\mu\frac{v}{r}\right)-\frac{2}{3}r\frac{Ma}{Re}\frac{\partial}{\partial r}\left(\mu\frac{v}{r}\right)\\ u\tau_{zr}+v\tau_{rr}-q_r-\tilde{\tau}\end{bmatrix}$$

The stress and heat flux terms are defined as follows:

$$q_r=k\frac{\partial T}{\partial r} \qquad q_z=k\frac{\partial T}{\partial z}$$

$$\tau_{zz}=\frac{2}{3}\frac{Ma}{Re}\mu\left(2\frac{\partial u}{\partial z}-\frac{\partial v}{\partial r}\right)$$

$$\tau_{rr}=\frac{2}{3}\frac{Ma}{Re}\mu\left(2\frac{\partial v}{\partial r}-\frac{\partial u}{\partial z}\right)$$

$$\hat{\tau}=\frac{2}{3}\frac{Ma}{Re}\mu\left(2\frac{v}{r}-\frac{\partial u}{\partial z}-\frac{\partial v}{\partial r}\right)$$

$$\tau_{zr}=\tau_{rz}=\frac{Ma}{Re}\mu\left(\frac{\partial u}{\partial r}+\frac{\partial v}{\partial z}\right)$$

$$\tilde{\tau}=\frac{2}{3}\frac{Ma}{Re}\mu\frac{v^2}{r}+\frac{2}{3}\frac{Ma}{Re}r\frac{\partial}{\partial r}\left(\mu\frac{v^2}{r}\right)+\frac{2}{3}\frac{Ma}{Re}r\frac{\partial}{\partial z}\left(\mu\frac{uv}{r}\right)$$

The viscosity is calculated using Sutherland's law

$$\mu=T^{3/2}\left(\frac{1+110.4/T_e}{T+110.4/T_e}\right)$$

The above equations represent the conservation of mass, momentum and total energy of Newtonian fluid motion. The variables ρ, u, v, P, t and E represent the density, velocity components in the z and r axis, pressure, time and total internal energy respectively. The characteristic length, velocity and density scales are listed in the nomenclature. The time scale is a combination of D_e / a_e while the pressure, viscosity and total energy scales are both defined in terms of $\rho_e a_e^2$.

Assuming a polytropic gas, the pressure and total internal energy are related by the equation of state. The temperature can be then calculated from the non-dimensionalised ideal gas law:

$$P=(\gamma-1)\left(E-\frac{1}{2}\rho(u^2+v^2)\right) \qquad P=\frac{\rho T}{\gamma}$$

The Navier-Stokes equations are solved using a total variation diminishing (TVD) version of Roe's approximate Riemann solver developed by Yee (1987). The numerical scheme is based on the second version of Godunov's method. A fourth order Runge-Kutta scheme is used to advance the solution in time with the time step size defined by the Courant condition.

A Lagrangian description of the particle motion is employed. The assumptions of the model used by Sommerfeld (1994) requires that:

- The particles do not interact or collide with each other
- The particles are perfect spheres with uniform material properties

Denoting each particle location by $z_{pk}(t)$, $r_{pk}(t)$ the equations governing the particle dynamics are

$$\frac{dU_k}{dt}=I_k \qquad U_k=\begin{bmatrix} z_p \\ r_p \\ u_p \\ v_p \\ T_p \end{bmatrix} \qquad I_k=\begin{bmatrix} u_p \\ v_p \\ A_p(u-u_p) \\ B_p(v-v_p) \\ B_p(T-T_p) \end{bmatrix}$$

$$A_p=\frac{3}{4}\Delta\bar{t}\,\frac{\bar{\rho}}{\bar{\rho}_p\bar{d}_p}C_D \qquad B_p=6\frac{\bar{C}_p}{\bar{C}_g}\frac{\bar{\mu}}{\bar{\rho}_p\bar{d}_p^2}\frac{Nu}{Pr}$$

where dimensionless variables are used unless it has an overbar.

Each computational 'parcel' represents a number of particles and is labelled by subscript k. The particles within the parcels are approximated to have the same velocity and temperature. The non-dimensional variables u_p, v_p and T_p represent the particle velocity components parallel to the z and r axes, and the temperature respectively. The drag coefficent C_D and Nusselt number Nu are estimated using empiricial formulas from Henderson (1976).

$$C_{D0}=\frac{24}{Re_k}\left(1+\frac{1}{6}Re_k^{2/3}\right) \qquad \text{if Re < 1000}$$

$$C_{D0}=0.44 \qquad \text{if Re > 1000}$$

$$Nu=2+0.6\sqrt{Re_k}\,Pr^{2/3} \qquad \text{Pr = 0.71 for air}$$

$$Re_k=\frac{\bar{\rho}_p\bar{d}_p\left|\bar{u}_k-\bar{u}_{pk}\right|}{\bar{\mu}} \qquad Pr=\frac{\bar{\mu}\,\bar{C}_g}{\bar{\kappa}}$$

In the case of large particle slip, compressibility effects contribute to an increase in particle drag and a modified drag coefficient from Carlson and Hoglund (1964) is used.

$$C_D=C_{D0}\left(1+\exp(-0.427/Ma_k^{4.63}-3/Re_k^{0.88})\right)$$

$$Ma_k=\frac{\left|\bar{u}_k-\bar{u}_{pk}\right|}{\bar{a}_k}$$

To account for the particle gas interaction an extra term S_p is added in the Navier-Stokes equations.

$$\frac{\partial U}{\partial t}+\frac{\partial F}{\partial z}+\frac{\partial G}{\partial r}+\frac{\partial F_v}{\partial z}+\frac{\partial G_v}{\partial r}+S+S_v+S_p=0$$

$$S_p=\begin{bmatrix} 0 \\ S_{pz} \\ S_{pr} \\ u_pS_{pz}+v_pS_{pr}+H_p \end{bmatrix}$$

The terms S_{px}, S_{py} and H_p are obtained by summation of all the parcels k contained within the dimensional grid volume $V_{i,j}$.

$$S_{pz}=\frac{\pi D_e}{8V_{i,j}}\sum_k \rho_k d_p^2 N_k C_{Dk}(u_k-u_{pk})\left|u_k-u_{pk}\right|$$

$$S_{pr}=\frac{\pi D_e}{8V_{i,j}}\sum_k \rho_k d_p^2 N_k C_{Dk}(v_k-v_{pk})\left|v_k-v_{pk}\right|$$

$$H_p=\frac{\pi D_e}{8V_{i,j}\rho_e a_e^3}\frac{\mu C_p}{Pr}\sum_k Nu_k d_p N_k (T_k-T_{pk})$$

The number of particles within each parcel N_k at the injection point can be found from:

$$N_k = \frac{6}{\pi}\frac{\eta \rho_e u_e \Delta A_j}{N_p \rho_p d_p^3}\Delta t$$

where N_p denotes the number of particles parcels injected per grid.

Figure 2 shows the computational domain used in the simulations. The adiabatic no slip wall boundary conditions are applied along the nozzle walls (GA and AB) and the substrate (DE) while a symmetry condition is imposed on the jet centerline (CD). For the far fields, (EF and FG) a non-reflecting boundary condition proposed by Toro (1999) is used. The gas condition at the nozzle exit (BC) is calculated assuming one-dimensional isentropic flow through the nozzle. The particle velocity and temperature at the nozzle exit is found by tracking a single parcel injected at the nozzle inlet at 3 m/s and 300 K. A log-normal size distribution assumed with standard deviation of $\sigma^2 = 0.25$.

$$f(d_p) = \frac{1}{\sqrt{(2\pi\sigma^2)}d_p}\exp\left(\frac{-(\ln d_p - \ln d_m)^2}{2\sigma^2}\right)$$

A random number [0, 1] is generated and the diameter obtained by reading off the cumulative probability distribution. Once the exit velocity and temperature are known, the parcels are randomly injected across 80% of the throat area for the two-phase simulation. The parcels are removed from the computational domain after passing through the substrate.

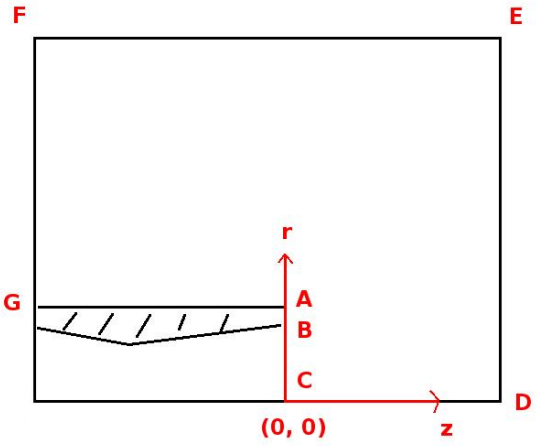

Figure 2: Schematic of computational domain.

The particle density and specific heats are 8960 kg/m^3 and 305 J/kg-K respectively. The particle loading ratio, defined as the ratio of the particle and gas mass flow rate, was set to 0.1.

RESULTS AND DISCUSSION

To assess the accuracy of the gas dynamic simulation, the jet centerline velocity for an overexpanded impinging jet is compared with PIV measurements by Jinglei (2006). It can be seen from Figure 3 that the computed results are agreeable with those obtained experimentally. Attempts at measuring the particle velocity using laser diagnostic techniques such as PIV have been made recently. Pattison et al. (2008) claim to have measured particle speeds as high as 900 m/s using a 16 x 16 pixel (3.5mm x 3.5mm) interrogation window size with a time interval of 4 microseconds between each image pair. This implies the particle travels a distance of 4 x 10^{-6} x 900 = 3.6 mm between each laser illumination. However, PIV analysis requires that the particles do not travel more than 25 % of the interrogation window length between each laser pulse (Raffel, Willert and Kompenhans (1999)). Hence the results are unlikely to be reliable.

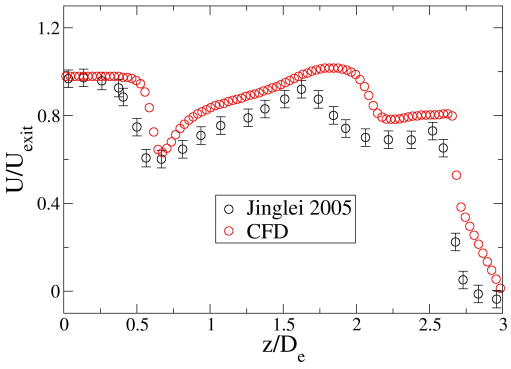

Figure 3: Jet centerline velocity for an overexpanded impinging air jet: PR = 0.63, Ma = 2.1.

The effect of the grid resolution and domain size on the simulation is examined by comparing the non-dimensional distance of the bow shock from the nozzle exit. The results are summarised in Table.1 and 2 respectively. The domain size is changed by increasing the length of GA and FG while the cell size is uniformly decreased. A maximum variation of 2% occurs in the bow shock distance as a result of different domain and cell size.

Table 1: Effect of domain size on bow shock distanc

	2D	3D	4D	FG
2D	1.842	1.851	1.849	
3D	1.847	1.836	1.841	
4D	1.839	1.844	1.840	
GA				

Table 2: Effect of cell size on bow shock distance.

Δ z, r				
0.010	0.020	0.030	0.040	0.050
1.844	1.842	1.845	1.851	1.932

In the present numerical investigation, a cell size of 0.03 is used with lengths GA and FG being $2D_e$ and $3D_e$ respectively. Eight particle parcels are injected per grid at each 0.01 non-dimensional time step. The particle data extracted at a point includes all parcels contained within a cell centered at that point of length $0.003D_e$.

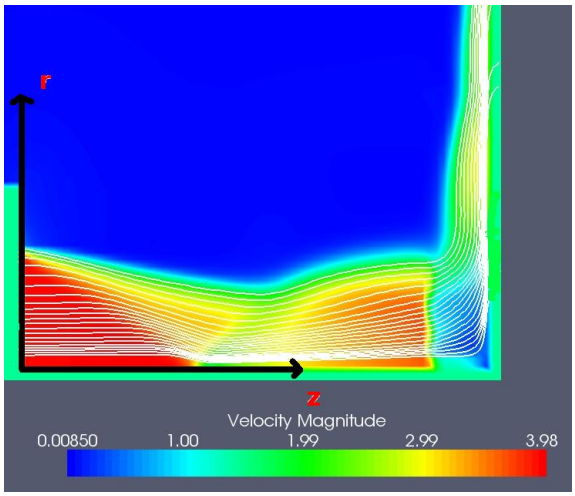

Figure 4: Non-dimensionalised gas velocity contour plot with particles of St = 17.2.

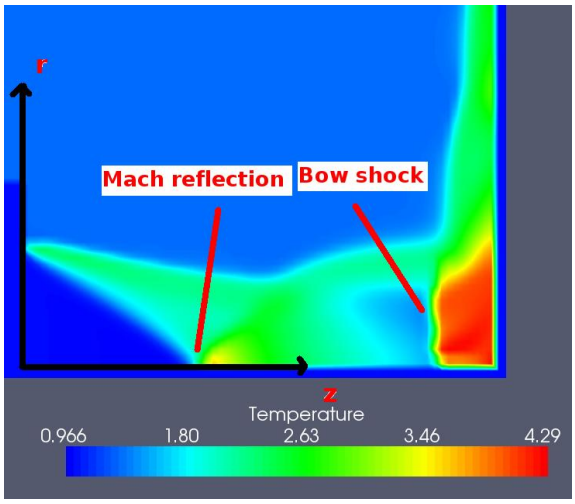

Figure 5: Non-dimensionalised gas temperature contour plot with particles of St = 17.2.

The velocity and temperature contours (Figures 4 and 5) of the supersonic impinging gas jet clearly show a region of stagnant fluid at high temperature prior to impingement. In previous simulations using the commercial software FLUENT, the occurrence of a recirculation bubble between the bow shock and substrate was observed. It has been noted by various researchers (Alvi and Iyer (1999)) that the existence of the bubble accompanied by an annular peak in the surface pressure distribution. The adverse pressure gradient due to the peak causes the boundary layer to separate along the substrate and approximately defines the size of the bubble. In the current simulation, a favorable pressure gradient was observed along the substrate with the flow remaining fully attached as illustrated by the streamlines in Figure 4.

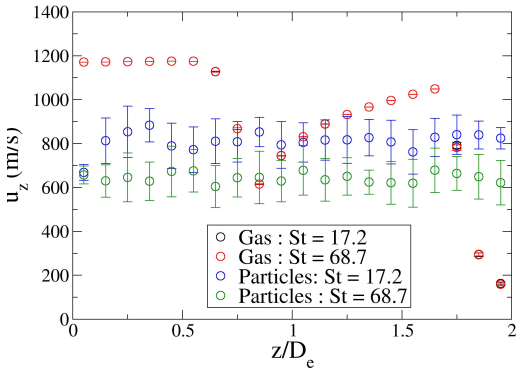

Figure 6: Jet centerline axial velocity profile.

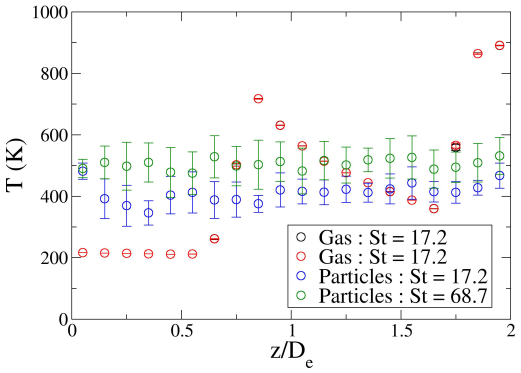

Figure 7: Jet centerline temperature profile.

Figures 6 and 7 shows the particle and gas velocities and temperatures along the jet centerline. The 'error bars' represents one standard deviation from the mean values. The carrier gas experiences a sudden drop in velocity (z/D_e ~ 0.8) from 1200 m/s to 600 m/s followed by a gradual acceleration to 1000 m/s prior to the bow shock at z/D_e ~ 1.6. The reverse trend is observed in the gas temperature which increases from 200 K to 700 K at the Mach reflection before cooling down again to 300 K at the bow shock. After the bow shock, the gas comes to rest at the substrate while reaching temperatures almost as high as that in the nozzle chamber. The change in gas velocity and temperature due to the presence of different sized particle is negligible. Despite the rapid change in the gas dynamics at z/D_e

~ 0.7 and 1.7, the particles' velocity and temperature remain relatively constant during the flight between the nozzle exit and substrate. This is consistent with the commonly accepted criteria (Raffel, Willert and Kompenhans (1999)) that for particles to responds to rapid changes in the flow, the Stokes number must be much less than one.

Schmidt et al. (2006) have investigated the particle bonding mechanism during cold spray and proposed a region of optimum particle impact conditions as shown in Figure 8. Ideally the impact velocity should fall between the critical and erosion velocity curves. The impact temperature is also important because if it is too low the brittle behaviour of the material reduces the particle deposition. For the present nozzle operating conditions, the impact velocities and temperatures for 4, 8, 11, 14, 17, 20 μm copper and aluminium particles are plotted in Figure 9. With both materials, the impact velocity decreases with increasing temperature and particle size in support of Schmidt's model. By varying the nozzle operating conditions and examining the coating quality for different particle-substrate combination and particle sizes, it is potentially possible to determine the optimal impact conditions.

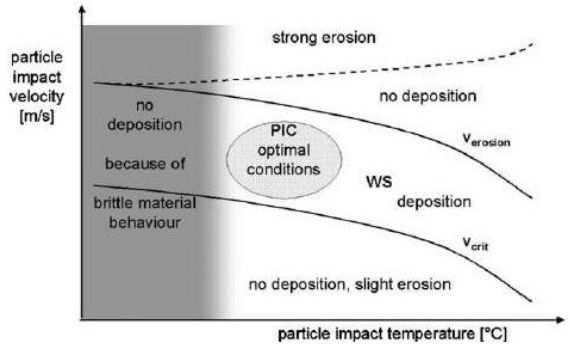

Figure 8: Optimum impact conditions for cold spraying. Schmidt et al. (2006)

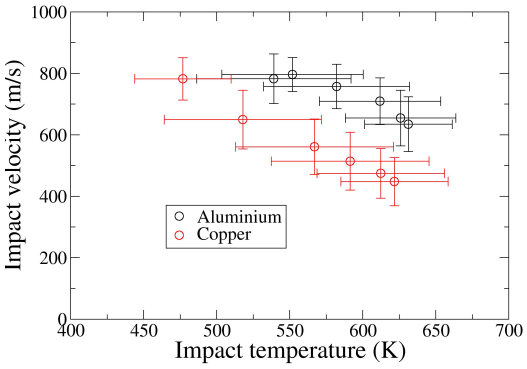

Figure 9: Particle impact velocity and temperature for Al and Cu particles in the range of 4- 20 μm.

CONCLUSION

An in-house Riemann solver coupled with Lagrangian particle tracking model has been successfully developed and benchmarked against experimental data. It has been shown in the present study that the presence of a Mach reflection and bow shock within the impinging gas jet has minimal influence on the particle velocity and trajectory given the Stokes number is much greater than one. The potential application of CFD in the finding the optimum impact conditions was also demonstrated.

REFERENCES

ALKIMOV, A.P., KOSAREV, V.F., NESTEROVICH, N.I. and PAPYRIN, A.N., (1990), "Method of cold spraying", Russian Patent No.1618778, Sept 8.

YEE, H.C., (1987), "Construction of explicit and implicit symmetric TVD schemes and their applications", *J. Comput. Phys.,* **68**, 151–179.

SOMMERFELD, M., (1994), "The structure of particle-laden, underexanded free jets", *Shock waves*, **3**, 299-311.

HENDERSON, C. B., (1976) "Drag coefficient of spheres in continuum and rarefied flows", *AIAA. J.*, **14:6**, 707-708.

CARLSON, D.J. and HOGLUND, R.F., (1964) "Particle drag and heat transfer in rocket nozzles", *AIAA. J.*, **2:11**, 1980-1984.

PATTISON, J., CELOTTO, S., KHAN, A. and O'NEILL, W., (2008), "Standoff distance and bow shock phenomena in the cold spray process", *Surf. Coat. Technol.,* **202**, 1443-1454.

SCHMIDT, T., GARTNER, F. and ASSADI, H. and KREYE, H., (2006)., ¨Development of a generalized parameter window for cold spray deposition", *Acta Mater.,* **54**, 729-742.

ALVI, F.S. and IYER, K.G., (1999), "Mean and unsteady flowfield properties of supersonic impinging jets with lift plates", *AIAA paper*, **99-1829**, 1–12.

TORO, E.F., (1999), " Riemann solvers and numerical methods for fluid dynamics", 2nd edition.

RAFFEL, M., WILLERT, C. and KOMPENHANS, J., (1998), "Particle image velocimetry", 2nd edition.